Design and Analysis of a New HTS Axial-Field Flux-Switching Machine

Yubin Wang, Mu Chen, T. W. Ching, *Senior Member, IEEE*, and K. T. Chau, *Fellow, IEEE*

***Abstract*—This paper proposes a new high-temperature superconductor (HTS) axial-field flux-switching machine with the merit of high power density for wind energy conversion. The key is to introduce a kind of modular racetrack cooling Dewar with static seals to replace the one with dynamic seals used in the conventional rotor excitation HTS machine. Also, the effects of rotor relative positions of the proposed machine on the back electromotive force are discussed. By using finite-element analysis, the machine performances are analyzed. Hence, the validity of the proposed machine is verified.**

***Index Terms*—Axial-field flux-switching machine, cooling Dewar, finite-element analysis (FEA), high-temperature superconductor, wind energy conversion.**

I. Introduction

In THE LAST decades, there are ever-increasing concerns on the applications of high-temperature superconductor (HTS) machines in many areas, such as warship drive, aerospace and wind power conversion, since they offer the merits of high power density and high efficiency [1]–[5]. Generally, for the HTS rotating machines, its HTS excitation windings which are fixed by non-magnetic materials locate on the rotor whereas the copper materials are used in armature windings. Thus, this kind of machines can be classified as rotor excitation HTS machines. Since both the HTS excitation windings and the rotor revolve around the shaft, this kind of machine configuration inevitably leads to high difficulty in the rotating seals of the cooling Dewar, hence increasing the machine cost.

Recently, a new class of stator excitation HTS machines with radial magnetic field, were proposed and investigated to change the rotating seal of the cooling Dewar to a static one [6]–[11]. For this kind of machines, since the HTS field-windings are located in the stator, it is much easier for refrigeration design than its rotor excitation counterpart. Moreover, since the cooling Dewar can be embedded into the stator core completely, the length of the airgaps is significantly reduced, hence increasing the magnetic loadings of the machines. Accordingly, the power density of HTS machines can greatly be improved.

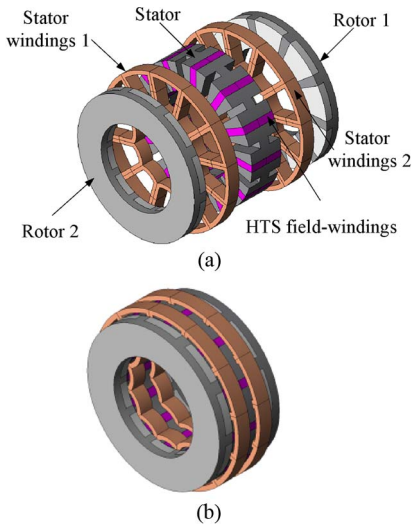

Fig. 1. HTS-AFSM configuration: (a) Exploded view and (b) Assembly view.

Several axial-field machines [12]–[14] are being exploited recently due to their high power densities and superior torque performances. Borrowing the idea of offering excitation field by using HTS field-windings located in the stator, a new HTS axial-field flux-switching machine (HTS-AFSM) is proposed and investigated for application to wind power generation. For the proposed machine, the BSCCO-2223 HTS tape is utilized as the field excitation windings under the temperature conditions of 30 K. In Section II, the machine configuration and its operation principle will be discussed. Then, Section III will focus on the design of cooling Dewar to accommodate the HTS windings. Next, Section IV will be devoted to using finite element analysis (FEA) for machine performance analysis. Finally, conclusion will be drawn in Section V.

II. Machine Configuration and Operation Principle

A. Machine Configuration

Fig. 1 shows the configuration of the proposed HTS-AFSM, which consists of two coaxial rotors with 10 salient poles and a stator with 12 poles. Each rotor is made of silicon steel sheet, without having any windings or magnets. The HTS windings and armature copper windings are all mounted on the stator which is sandwiched between rotor 1 and rotor 2. As shown in Fig. 1(a), the HTS field-excitation windings, which are

Manuscript received July 29, 2014; accepted October 21, 2014. Date of publication November 3, 2014; date of current version January 16, 2015. This work was supported in part by a grant (Project no. 51277183) from the National Natural Science Foundation of China, by a grant (Project no. 2013CB035603) from the National Key Basic Research Program of China, and by a grant from the Fundamental Research Funds for the Central Universities (Project no. 14CX02085A) of China.

Y. Wang is with the College of Information and Control Engineering, China University of Petroleum, Qingdao 266555, China (e-mail: yubwang5190@163.com).

M. Chen and K. T. Chau are with the Department of Electrical and Electronic Engineering, The University of Hong Kong, Pokfulam, Hong Kong.

T. W. Ching is with the Faculty of Science and Technology, University of Macau, Macau, China.

Color versions of one or more of the figures in this paper are available online at http://ieeexplore.ieee.org.

Digital Object Identifier 10.1109/TASC.2014.2366465

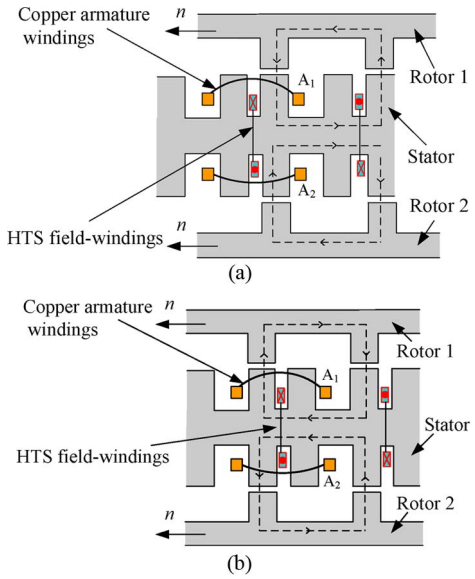

Fig. 2. Operation principle: (a) Excitation flux approaching armature windings and (b) Excitation flux leaving armature windings.

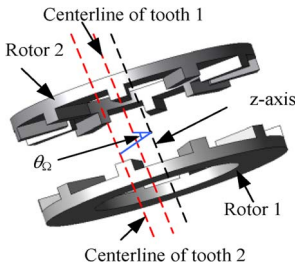

Fig. 3. Mechanical angle between centerlines along circumferential direction.

immersed in the cooling Dewar, are embedded into the stator completely. It means that HTS-AFSM offers the merit of shorter airgap lengths than its rotor excitation counterpart. Fig. 1(b) shows the assembly diagram of the proposed HTS-AFSM.

B. Operation Principle

Fig. 2 shows two special positions between the both two rotating rotors and the stationary stator, where the peak values of flux linkage of both armature windings A_1 and A_2 can be obtained. According to the principle of minimum magnetic reluctance, when the rotors move to the position as shown in Fig. 2(a), the excitation flux, which is excited by HTS field-windings, approaches the armature windings of both A_1 and A_2 via the airgap, and increases to the positive maximum value. On the contrary, when the rotors move to the position as shown Fig. 2(b), the excitation flux leaves the armature windings, and decreases to the negative maximum value. Namely, the rotational movement through a rotor pole pitch causes 360° (electrical) change of EMF of both the armature windings A_1 and A_2.

It should be noted that the center lines of teeth of rotor 1 are aligned with those of rotor 2 as shown in Fig. 2. Therefore, the maximum value of the sum of flux linkage of both the windings A_1 and A_2 can be obtained. On the other hand, when the relative positions of center lines have been changed along with the circumferential direction as shown in Fig. 3, where θ_Ω is the mechanical angle between the center lines, the value of this sum will be altered since the phase difference of flux linkage between windings A_1 and A_2 has been changed although the peak value of flux linkage of each winding remains unchanged. Thus, the sum of back EMF of the two windings, which is induced from the variation of flux linkage, will vary with the alteration of relative positions between rotor 1 and rotor 2.

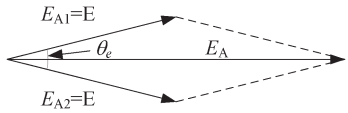

Fig. 4. Vector diagram of EMF from both armature windings.

TABLE I
BACK EMF UNDER VARIOUS PHASE DIFFERENCES

θ_e	E_A
0^0	2.00E
20^0	1.97E
40^0	1.88E
60^0	1.73E
80^0	1.53E
100^0	1.29E
120^0	1.00E
140^0	0.69E
160^0	0.35E
180^0	0

Fig. 5. Arrangement of cooling Dewars of the proposed machine.

Fig. 4 illustrates the vector sum of the back EMF of both windings A_1 and A_2, where θ_e is the phase difference of back EMF between the two windings, E is the peak value of back EMF of each winding, E_A is the vector sum of back EMF of both windings A_1 and A_2 respectively. According to Fig. 4, the vector sum of back EMF under the condition of various phase differences is calculated and listed in Table I. It can be found that the back EMF of the armature windings is dominated by the relative position between the two rotors.

III. DESIGN OF COOLING SYSTEM

Other than the cylindrical cooling Dewar used in rotor excitation HTS machine, a new kind of modular racetrack cooling Dewar is proposed in this paper to achieve static seal of the rotating HTS machine. Since the proposed machine equips with 12 HTS field-windings, the cooling system possesses the same number of racetrack Dewars. Fig. 5 shows the arrangement of cooling Dewars of the proposed machine. It can be found that the 12 cooling Dewars can be embedded into the stator core completely. The cryogenic liquid nitrogen, which is fuelled by the cryogenic containers, is shunt into 12 branches via a main inflow channel and flow into corresponding racetrack cooling

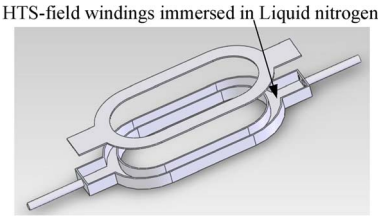

Fig. 6. Configuration of inner Dewar.

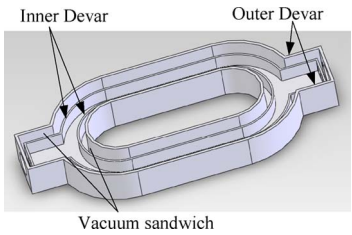

Fig. 7. Inner Dewar putting into the outer Devar.

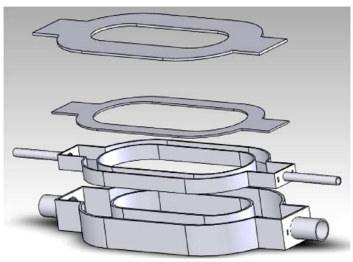

Fig. 8. Exploded view of cooling Dewar.

TABLE II
KEY DATA OF HTS-AFSM MACHINE

Parameters	HTS-AFSM
Number of rotor poles	10
Number of stator poles	12
Stator outside diameter (mm)	400
Stator inside diameter (mm)	240
Rotor outside diameter (mm)	400
Rotor inside diameter (mm)	240
Stack length (mm)	100
Rotor 1 length (mm)	40
Rotor 2 length (mm)	40
Airgap length (mm)	1
Number of phases	3
Rated speed (rpm)	60
HTS material	Bi-2223

Dewars to cool the HTS field-windings. Then, the cryogenic liquid nitrogen, which outflows from the cooling Dewars, converges on a main collection channel and return to the aforementioned cryogenic containers for the purpose of heat exchange.

To keep the operation temperature of the HTS field-windings at 30 K, a novel cooling Dewar system has been designed. Fig. 6 shows the configuration of inner Dewar of the cooling Dewar, where the HTS field-windings are immersed here with cryogenic liquid nitrogen. After winding and fixing of the HTS field-windings, the inner Dewar is wrapped with insulation material on its outer surface. As shown in Fig. 7, the polytetrafluoroethylene (PTFE) supports are placed between the inner and outer Dewars to form the vacuum sandwich structure so that the heat insulation can be achieved effectively. Fig. 8 depicts the exploded view of a complete cooling Dewar system.

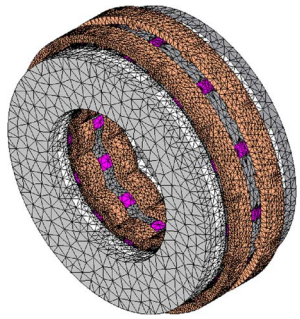

Fig. 9. 3D mesh of HTS-AFSM.

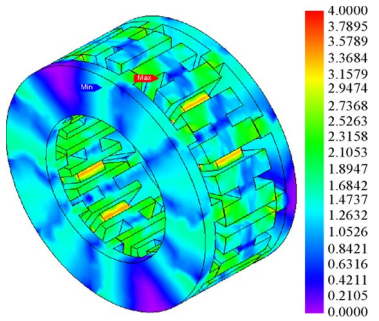

Fig. 10. Distribution of flux density of HTS-AFSM.

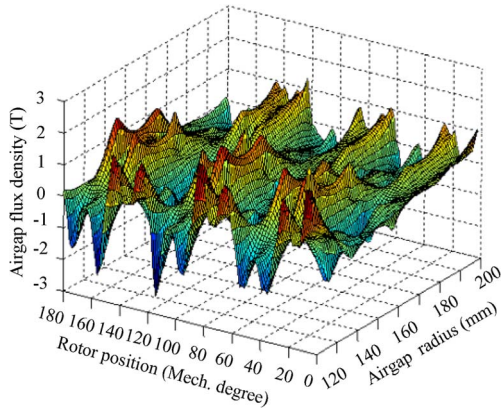

Fig. 11. Distribution of airgap flux density of HTS-AFSM.

IV. ELECTROMAGNETIC PERFORMANCE ANALYSIS

To verify the validities of the proposed machine, its electromagnetic performances are analyzed by using 3D-FEA. The key design data of the proposed machine are summarized in Table II.

Fig. 9 shows the 3D finite element mesh model of the proposed machine. Fig. 10 depicts the distribution of flux density in both stator and rotor cores with the excitation current of 100A/turn. In the stator yoke, its maximum magnetic flux density is up to 3.4 T since the BSCCO-2223 HTS field-windings can offer higher current than that of conventional copper field-windings with the same number of winding turns. On the other hand, from an efficiency point of view, since the proposed machine operates at a relatively low speed, its iron losses are acceptable hence ensuring the efficiency of the machine.

Fig. 11 depicts the distributions of the airgap flux density along the circumferential direction when the phase difference

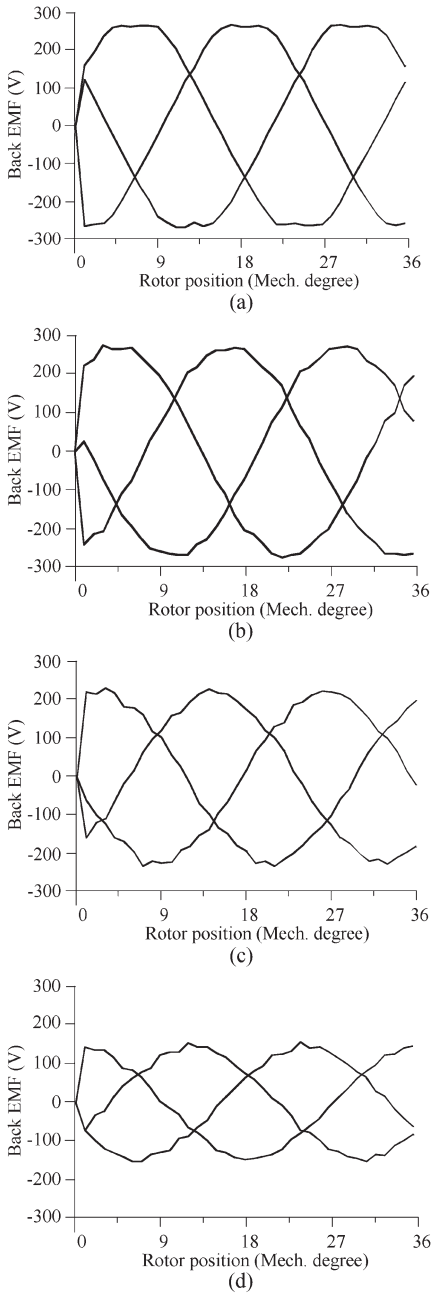

Fig. 12. Back EMF waveforms of HTS-AFSM with different phase difference θ_e at speed of 60 rpm: (a) $\theta_e = 0°$, (b) $\theta_e = 40°$, (c) $\theta_e = 80°$, and (d) $\theta_e = 120°$.

θ_e equals to 0^0. It can be found that the airgap flux density varies on a saddle surface within an electrical period. Also, when the airgap radius falls within the range of 170 mm to 190 mm, the peak value of airgap flux densities is the lowest. It can be explained by the difference of the rate of change of tooth width of both the stator and rotor in the circumferential direction as resulted from the difference of pole numbers of both the stator and rotor. Therefore, the distribution of airgap flux density can be improved by increasing the diameter and pole numbers of both the stator and rotor.

Based on the distribution of the airgap flux density, the back EMFs with different phase difference θ_e can be calculated and illustrated in Fig. 12. In Fig. 12(a), the phase difference θ_e is zero, thus, the peak value of the back EMF of the armature windings reaches its maximum value. Fig. 12(b)–(d) depict the back EMF waveforms when the rotor 1 counterclockwise rotate 40°, 80°, and 120° electrical angle respectively. It can be found that the peak values of the back EMF decrease with the increase of phase difference θ_e whereas the phase advance angle of back EMF emerges gradually. Compared with Table I, it can be found that the FEA results agree well with the calculated values, hence verifying the validity of theoretical analysis. On the other hand, the total harmonic distortion (THD) of back EMF varies from 2.49% to 3.96% as illustrated in Fig. 13 while the two rotors are regulated with different rotor relative positions. It reveals that the THD of back EMF is low and acceptable. It should be noted that this feature of adjustable back EMF of the machine can be utilized as an additional auxiliary measure to keep the output voltage constant when the HTS field-excitation current controller failed to work under time-varying wind speed.

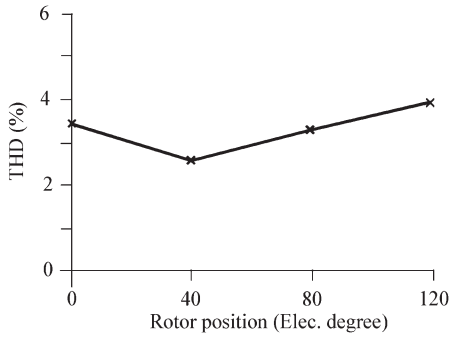

Fig. 13. THD of back EMF of HTS-AFSM with different phase difference θ_e.

V. Conclusion

In this paper, a new HTS-AFSM, adopting BSCCO-2223 HTS tape windings for field excitation, has been proposed for the wind power generation system. The machine configuration, operation principle, and design of modular racetrack cooling Dewar system have been discussed. By using 3D-FEA, the electromagnetic properties of the proposed machine have been analyzed. Moreover, a new method, which regulates the back EMF by adjusting the rotor relative positions, is proposed to keep the output voltage of the machine constant when the HTS field-excitation current controller failed under time-varying wind speed. By assessing the machine performances, the validity of the proposed machine is verified.

References

[1] D. U. Gubser, "US Navy's superconductivity programs scientific curiosity to fleet utility," *IEEE Trans. Appl. Supercond.*, vol. 21, no. 3, pp. 931–935, Jun. 2011.

[2] B. Gamble, G. Snitchler, and T. MacDonald, "Full power test of a 36.5 MW HTS propulsion motor," *IEEE Trans. Appl. Supercond.*, vol. 21, no. 3, pp. 1083–1088, Jun. 2011.

[3] L. G. Yan, "Recent progress of superconducting magnet technology in China," *IEEE Trans. Appl. Supercond.*, vol. 20, no. 3, pp. 123–134, Jun. 2010.

[4] J. B. Song *et al.*, "HTS wind power generator: Electromagnetic force between no-insulation and insulation coils under time-varying conditions," *IEEE Trans. Appl. Supercond.*, vol. 24, no. 3, Jun. 2014, Art. ID. 5201005.

[5] K. Sivasubramaniam *et al.*, "Development of a high speed HTS generator for airborne applications," *IEEE Trans. Appl. Supercond.*, vol. 19, no. 3, pp. 1656–1661, Jun. 2009.

[6] Y. B. Wang, J. X. Sun, Z. X. Zou, Z. Wang, and K. T. Chau, "Design and analysis of a HTS flux-switching machine for wind energy conversion," *IEEE Trans. Appl. Supercond.*, vol. 23, no. 3, Jun. 2013, Art. ID. 5000904.

[7] Q. Chen, G. H. Liu, Z. M. Liu, and X. H. Li, "Design and analysis of a new fully stator-HTS motor," *IEEE Trans. Appl. Supercond.*, vol. 24, no. 3, Jun. 2014, Art. ID. 5202005.

[8] R. Shafaie and M. Kalantar, "Design of a 10-MW-class wind turbine HTS synchronous generator with optimized field winding," *IEEE Trans. Appl. Supercond.*, vol. 23, no. 4, Aug. 2013, Art. ID. 5202307.

[9] W. O. S. Bailey, Y. Yang, C. Beduz, and K. F. Goddard, "Short circuit tests on a coreless HTS synchronous generator," *IEEE Trans. Appl. Supercond.*, vol. 23, no. 3, Jun. 2013, Art. ID. 5201505.

[10] C. Liu, K. T. Chau, J. Zhong, and J. Li, "Design and analysis of a HTS brushless doubly-fed doubly-salient machine," *IEEE Trans. Appl. Supercond.*, vol. 21, no. 3, pp. 1119–1122, Jun. 2011.

[11] J. G. Li and K. T. Chau, "A novel HTS PM vernier motor for direct-drive propulsion," *IEEE Trans. Appl. Supercond.*, vol. 21, no. 3, pp. 1175–1179, Jun. 2011.

[12] M. Y. Lin, L. Hao, X. Li, X. M. Zhao, and Z. Q. Zhu, "A novel axial field flux-switching permanent magnet wind power generator," *IEEE Trans. Magn.*, vol. 47, no. 10, pp. 4457–4460, Oct. 2011.

[13] L. Hao *et al.*, "Novel dual-rotor axial field flux-switching permanent magnet machine," *IEEE Trans. Magn.*, vol. 48, no. 11, pp. 4232–4235, Nov. 2012.

[14] C. H. T. Lee, C. Liu, and K. T. Chau, "A magnetless axial-flux machine for range-extended electric vehicles," *Energies*, vol. 7, no. 3, pp. 1483–1499, Mar. 2014.